Wave-vector-dependent exchange interaction and its relevance for the effective exciton mass in Cu_2O

G. Dasbach,* D. Fröhlich, R. Klieber, D. Suter, and M. Bayer
Institut für Physik, Universität Dortmund, D-44221 Dortmund, Germany

H. Stolz
Fachbereich Physik, Universität Rostock, D-18051 Rostock, Germany
(Received 17 February 2004; published 27 July 2004)

The wave-vector dependence of electron-hole exchange interaction is investigated. For the yellow 1S exciton in Cu_2O the exchange is derived up to the order k^2. The theoretical predictions are verified experimentally by high-resolution absorption experiments. In agreement with theory the fine structure shows a characteristic dependence on the direction of the wave vector. The exchange splitting of the orthoexciton triplet are distinguished from strain-induced perturbations. The exchange gives rise to an isotropic and an anisotropic correction of the effective exciton mass. This can explain the discrepancies in the measurements of the exciton mass in Cu_2O.

DOI: 10.1103/PhysRevB.70.045206 PACS number(s): 78.20.−e, 78.40.Fy, 71.35.Cc

I. INTRODUCTION

Spins are coupled via exchange interaction. While electron-electron exchange is well understood in atomic systems, the topic is of increased complexity for the electron-hole exchange interaction in semiconductors. Investigations of electron-hole exchange, beginning with bulk semiconductors,[1,2] have been extended to quantum wells[3] and, recently, also to quantum dots.[4] Nowadays efforts concentrate on spin phenomena in such micro- and nanostructures. However the understanding of electron-hole exchange even in bulk materials is far from being complete.

In semiconductors an excited electron in the conduction band couples to a hole in the valence band via Coulomb interaction. The properties of the coupled electron-hole pair are determined by the valence as well as the conduction band. One therefore expects that the electron-hole exchange interaction also depends on the full band structure and hence on the wave vector $\mathbf{k}$ of the exciton center-of-mass motion. Due to the complexity of the bands, difficulties in calculating the electron-hole exchange microscopically arise. Attempts to describe it on a quantitative level can hardly be found.[5,6] Exchange is normally approximated as a spin-spin interaction, which is independent of the wave vector in bulk materials. This isotropic approximation represents a severe simplification of the exchange interaction omitting much of the lattice properties. Nevertheless, these calculations are sufficient to describe the experiments reported so far. These studies, however, were performed with modest spectral resolution of typically $\gtrsim 20\ \mu$eV. Resolving the more complex nature of exchange is challenging.[7] Typically exchange splittings are small. Further, inhomogeneous and homogenous line broadening often mask the underlying fine structure.

The goal of the present study is to overcome these difficulties and to investigate electron-hole exchange for the example of the yellow 1S orthoexciton in Cu_2O. Cu_2O is the prototype material for exciton physics.[8] Because of its high crystal quality and large exciton binding energy of 150 meV, it is possible to observe several hydrogen-like exciton series. To minimize the effects of radiative broadening, we study the yellow 1S orthoexciton transition, which is dipole forbidden, but quadrupole allowed. This extremely sharp exciton transition is ideally suited for the study of electron-hole exchange and its wave-vector dependence.

Besides the requirements on the sample side, the experimental setup has to provide an adequate spectral resolution. The $\mathbf{k}$-dependent exchange splitting is expected to be on the order of few μeV. Therefore, to monitor wave-vector-dependent energy shifts a resolution in the sub-μeV regime is required.

This paper is organized as follows. In Sec. II we will derive the exchange fine structure of the yellow 1S orthoexcitons in Cu_2O. This description is based on the theory of invariants and describes the wave-vector dependence of the exchange up to the order k^2. As our approach is not microscopic the absolute magnitude of the exchange remains to be determined. In Sec. III we will describe the experimental technique. Besides the setup, we will explain the essential steps of the sample preparation. This will be followed by the presentation of the experimental data, which will be compared to the theoretical predictions of Sec. II. In Sec. IV we evaluate to what extent our results can be affected by strain. This will be followed by a discussion of our results (Sec. V), where we focus on the influence of the exchange interaction on the effective exciton mass. In Sec. VI we present our conclusions.

II. THEORY

Cu_2O condenses in a cubic structure, where the copper ions form a face-centered sublattice, and the oxygen ions, a body-centered sublattice. The arrangement of both lattices is such that a copper ion is centered between two oxygen ions. This makes Cu_2O a simple cubic crystal with inversion symmetry, described by the point group O_h. The valence band of highest energy has Γ_7^+ symmetry, while the lowest conduc-

tion band has Γ_6^+ symmetry. The excitonic transitions with holes in the Γ_7^+ band and electrons in the Γ_6^+ band give the so-called yellow exciton series. Thus the yellow 1S excitons are the lowest excited state.

The exciton representation (Γ_{ex}) is obtained from the direct product of electron (Γ_e) and hole (Γ_h) representations and the envelope function ($\Gamma_{env}=\Gamma_1^+$). This gives for the yellow 1S excitons:[9]

$$\Gamma_{ex}=\Gamma_{env}\otimes\Gamma_e\otimes\Gamma_h=\Gamma_1^+\otimes\Gamma_6^+\otimes\Gamma_7^+=\Gamma_5^+\oplus\Gamma_2^+. \quad (1)$$

The threefold Γ_5^+ states are termed orthoexcitons, while the single Γ_2^+ level is referred to as paraexciton. In the following we will solely concentrate on the orthoexcitons, since the paraexciton is split off by $\Delta_0=12.1$ meV[14] and is optically forbidden to all orders. A more precise evaluation of this exchange splitting will be discussed elsewhere.

The transition from the ground state (Γ_1^+) to the 1S orthoexcitons (Γ_5^+) is dipole (Γ_4^-) forbidden as the dipole operator has odd symmetry ($\langle\Gamma_5^+|\Gamma_4^-|\Gamma_1^+\rangle=0$). In lowest order, the orthoexciton couples to light via quadrupole interaction $\Gamma_5^+(\langle\Gamma_5^+|\Gamma_5^+|\Gamma_1^+\rangle\neq 0)$. Unlike the dipole operator, the quadrupole operator depends on the direction of the light wave vector **k** and the polarization vector **e** relative to the lattice. Because of the **k** dependence the transition is anisotropic even in a cubic crystal. The amplitudes (QA_1 to QA_3) of the orthoexciton transitions are given by the symmetric vector product of **k** and **e**:[10]

$$\begin{pmatrix} QA_1 \\ QA_2 \\ QA_3 \end{pmatrix}=\begin{pmatrix} e_yk_z+e_zk_y \\ e_zk_x+e_xk_z \\ e_xk_y+e_yk_x \end{pmatrix}. \quad (2)$$

We now proceed with the derivation of the electron-hole exchange. Typically the theoretical treatment does not go beyond the **k**-independent terms, as this already agrees with the data reported so far. For our purposes such a treatment is insufficient and terms of higher order in **k** need to be taken into account. In the following we will develop the electron-hole exchange up to the order k^2.

In the most general case the exchange interaction J_{ex} for the charge distributions ρ and ρ' is given by:[1]

$$J_{ex}=\delta_{\mathbf{k},\mathbf{k}'}\sum_{\mathbf{R}}e^{i\mathbf{k}\cdot\mathbf{R}}\int\int\frac{\rho^*(\mathbf{r}_1)\rho'(\mathbf{r}_2)d\mathbf{r}_1d\mathbf{r}_2}{|\mathbf{r}_1-\mathbf{r}_2-\mathbf{R}|}, \quad (3)$$

with the lattice vectors **R** and the spatial vector **r**. The orthoexciton exchange is determined by the interaction of the spin-singlet exciton charge distributions, which are given by $\rho(\mathbf{r})=e\Sigma_{\mathbf{R}}\Psi(\mathbf{R})\Sigma_\sigma a(\mathbf{r})b(\mathbf{r}+\mathbf{R})^*$, whereby $a(\mathbf{r})$ and $b(\mathbf{r}+\mathbf{R})$ denote the conduction and valence band Wannier functions and Σ_σ denotes a summation over all spin states.[1]

Introducing the Fourier transform of the charge distributions

$$\mathcal{M}(\mathbf{k})=\int d\mathbf{r}\rho(\mathbf{r})\exp(-i\mathbf{k}\cdot\mathbf{r}), \quad (4)$$

the exchange integral is transformed into a sum over all reciprocal lattice vectors $\mathbf{K}_i$[1]

$$J_{ex}=\delta_{\mathbf{k},\mathbf{k}'}\frac{4\pi}{\Omega}\sum_i\frac{\mathcal{M}^*(\mathbf{k}+\mathbf{K}_i)\mathcal{M}'(\mathbf{k}+\mathbf{K}_i)}{(\mathbf{k}+\mathbf{K}_i)^2}. \quad (5)$$

The electron-hole exchange can be split into long-range (LR) and short-range (SR) contributions. Qualitatively, the SR exchange splitting of the excitons originates from the interactions between an electron and a hole located in the same unit cell, while the LR part originates from the interaction between an electron and a hole located in different unit cells.

A. Long-range exchange interaction

We define the quadrupole electron-hole LR exchange as the term with $\mathbf{K}_i=0$ in Eq. (5)

$$J_{ex}^Q=\delta_{\mathbf{k},\mathbf{k}'}\frac{4\pi}{\Omega}\frac{\mathcal{M}^*(\mathbf{k})\mathcal{M}'(\mathbf{k})}{k^2}, \quad (6)$$

and the SR part as all other terms with $\mathbf{K}_i\neq 0$. These definitions of the two exchange contributions are typically referred to as "nonanalytic" ($\mathbf{K}_i=0$) and "analytic" exchange ($\mathbf{K}_i\neq 0$). However, for higher orders of **k** the nonanalytic term becomes analytic. To avoid a contradictory nomenclature we use the nomenclature for the separation of the exchange contributions in real-space, long-range, and short-range exchange. Both definitions are very similar, however not identical.[4] We expand $\exp(-i\mathbf{k}\times\mathbf{r})$ in Eq. (4) into spherical harmonics $Y_{l,m}$

$$e^{-i\mathbf{k}\cdot\mathbf{r}}=\sum_{l=0}^{\infty}\sum_{m=-l}^{m=+l}4\pi(-i)^l j_l(kr)Y_{l,m}^*(\alpha,\beta)Y_{l,m}(\theta,\phi), \quad (7)$$

where θ, ϕ and α, β are the polar angles of **k** and **r** with respect to the x,y,z coordinate system (cubic axes), and $j_l(kr)$ is the modified Bessel function of order l. For $l=2$ it is given by $j_2(kr)=(kr)^2/15\ldots$, where we neglect higher order terms. Decomposing ρ into multipoles[11]

$$\rho_{l,m}=\int d\mathbf{r}r^l\sqrt{\frac{4\pi}{2l+1}}Y_{l,m}^*\rho(\mathbf{r}), \quad (8)$$

we find the quadrupole moments ($l=2$)

$$q_m=\sqrt{\frac{4\pi}{5}}\int d\mathbf{r}r^2Y_{2,m}^*\rho(\mathbf{r}). \quad (9)$$

Using Eqs. (4), (7), and (9) we get

$$\mathcal{M}(\mathbf{k})=\int d\mathbf{r}\rho(\mathbf{r})\sum_{m=-2}^{m=+2}4\pi(-i)^2j_2(kr)Y_{2,m}^*(\alpha,\beta)Y_{2,m}(\theta,\phi)$$
$$=-\sqrt{\frac{4\pi}{45}}k^2\sum_{m=-2}^{m=+2}q_mY_{2,m}(\theta,\phi). \quad (10)$$

Substituting Eq. (10) into Eq. (6) the LR quadrupole-quadrupole exchange is given by

$$J_{ex}^{Q} = \delta_{\mathbf{k},\mathbf{k}'} \frac{16\pi^2}{45\Omega} k^2 \sum_{m_{1,2}=-2}^{2} q_{m_1}^{*} q'_{m_2} Y_{2,m_1}^{*}(\theta,\phi) Y_{2,m_2}(\theta,\phi). \tag{11}$$

To explicitly calculate the exchange interaction, we take a look at the specific electron and hole charge distributions. For the yellow 1S orthoexciton in Cu_2O the spin-singlet part of the Wannier functions are written as $\phi_{c,s}$ for the conduction and $\phi_{v,yz}, \phi_{v,xz}, \phi_{v,xy}$ for the valence band, with *s*- and *d*-like character, respectively. Ortho- and paraexciton are not simple product forms of the pure electron ($|\uparrow_e\rangle, |\downarrow_e\rangle$) and hole spin states ($|\uparrow_h\rangle, |\downarrow_h\rangle$). The Γ_7^+ hole states ($|\uparrow_H\rangle, |\downarrow_H\rangle$) are linear combinations of $|\uparrow_h\rangle$ and $|\downarrow_h\rangle$:

$$|\uparrow_H\rangle = \frac{-\mathrm{i}}{\sqrt{3}}[(\phi_{v,yz} + \mathrm{i}\phi_{v,zx})|\downarrow_h\rangle + \phi_{v,xy}|\uparrow_h\rangle],$$

$$|\downarrow_H\rangle = \frac{-\mathrm{i}}{\sqrt{3}}[(\phi_{v,yz} - \mathrm{i}\phi_{v,zx})|\uparrow_h\rangle - \phi_{v,xy}|\downarrow_h\rangle]. \tag{12}$$

The singlet ($|S\rangle$) and the three triplet ($|T_{+1}\rangle, |T_{-1}\rangle, |T_0\rangle$) states are given by:

$$|S\rangle = \frac{1}{\sqrt{2}}(|\uparrow_e,\downarrow_h\rangle - |\downarrow_e,\uparrow_h\rangle),$$

$$|T_0\rangle = \frac{1}{\sqrt{2}}(|\uparrow_e,\downarrow_h\rangle + |\downarrow_e,\uparrow_h\rangle),$$

$$|T_{-1}\rangle = |\downarrow_e,\downarrow_h\rangle,$$

$$|T_{+1}\rangle = |\uparrow_e,\uparrow_h\rangle. \tag{13}$$

Using the singlet-triplet notation the paraexciton state ($|P\rangle$) and the three orthoexciton states ($|O_{yz}\rangle, |O_{zx}\rangle, |O_{xy}\rangle$) in the Cartesian Γ_5^+ basis can be written as

$$|P\rangle = \frac{\mathrm{i}}{\sqrt{6}}\phi_{c,s}[\phi_{v,yz}(|T_{-1}\rangle - |T_{+1}\rangle) + \mathrm{i}\phi_{v,zx}(|T_{-1}\rangle + |T_{+1}\rangle) + \sqrt{2}\phi_{v,xy}|T_0\rangle],$$

$$|O_{yz}\rangle = \frac{1}{\sqrt{6}}\phi_{c,s}[\sqrt{2}\phi_{v,yz}|S\rangle + \mathrm{i}\sqrt{2}\phi_{v,zx}|T_0\rangle + \phi_{v,xy}(|T_{+1}\rangle + |T_{-1}\rangle)],$$

$$|O_{zx}\rangle = \frac{-\mathrm{i}}{\sqrt{6}}\phi_{c,s}[\sqrt{2}\phi_{v,yz}|T_0\rangle + \mathrm{i}\sqrt{2}\phi_{v,zx}|S\rangle + \phi_{v,xy}(|T_{+1}\rangle - |T_{-1}\rangle)],$$

$$|O_{xy}\rangle = \frac{-1}{\sqrt{6}}\phi_{c,s}[\phi_{v,yz}(|T_{+1}\rangle + |T_{-1}\rangle) - \mathrm{i}\phi_{v,zx}(|T_{+1}\rangle - |T_{-1}\rangle) - \sqrt{2}\phi_{v,xy}|S\rangle]. \tag{14}$$

After having defined a proper basis, we now use the wavefunctions to calculate the LR exchange. As electron-hole exchange interaction affects states with opposite spin, only the singlet $|S\rangle$ terms contribute to the exchange splitting. From Eq. (14) we find that the paraexciton $|P\rangle$ is a pure triplet state and is thus not affected by the quadrupolar exchange. The quadrupole moments in the Cartesian basis are calculated from the singlet-charge densities using Eq. (14)

$$\rho_P(\mathbf{r}) = 0,$$

$$\rho_{yz}(\mathbf{r}) = \frac{1}{\sqrt{3}} e \phi_{c,s}\phi_{v,yz},$$

$$\rho_{zx}(\mathbf{r}) = \frac{1}{\sqrt{3}} e \phi_{c,s}\phi_{v,zx},$$

$$\rho_{xy}(\mathbf{r}) = \frac{1}{\sqrt{3}} e \phi_{c,s}\phi_{v,xy}. \tag{15}$$

The valence band Wannier functions are given by[11]

$$\phi_{v,yz} = d(r)\sin\theta\cos\theta\sin\phi = \mathrm{i}\sqrt{\tfrac{2\pi}{15}}d(r)(Y_{2,1} + Y_{2,-1}),$$

$$\phi_{v,zx} = d(r)\sin\theta\cos\theta\cos\phi = -\sqrt{\tfrac{2\pi}{15}}d(r)(Y_{2,1} - Y_{2,-1}),$$

$$\phi_{v,xy} = d(r)\sin^2\theta\cos\phi\sin\phi = -\mathrm{i}\sqrt{\tfrac{2\pi}{15}}d(r)(Y_{2,2} - Y_{2,-2}). \tag{16}$$

With Eqs. (15) and (16) we rewrite Eq. (9). Using the orthogonality relations of the spherical harmonics, one finds that $\phi_{v,yz}$, $\phi_{v,zx}$ contribute only to q_1 and q_{-1}, while $\phi_{v,xy}$ contributes to q_2 and q_{-2}. q_0 is always zero. Decomposing the quadrupole moments into contributions from the basis states $|O_{yz}\rangle$, $|O_{zx}\rangle$, $|O_{xy}\rangle$ we find

$$\begin{pmatrix} q_{+2} \\ q_{+1} \\ q_0 \\ q_{-1} \\ q_{-2} \end{pmatrix} = C_0 \left[\begin{pmatrix} 0 \\ \mathrm{i} \\ 0 \\ \mathrm{i} \\ 0 \end{pmatrix}_{|O_{yz}\rangle} + \begin{pmatrix} 0 \\ -1 \\ 0 \\ 1 \\ 0 \end{pmatrix}_{|O_{zx}\rangle} + \begin{pmatrix} -\mathrm{i} \\ 0 \\ 0 \\ 0 \\ \mathrm{i} \end{pmatrix}_{|O_{xy}\rangle} \right]. \tag{17}$$

All prefactors are included in C_0. We now express the LR exchange in matrix form in the $|O_{yz}\rangle$, $|O_{zx}\rangle$, $|O_{xy}\rangle$ basis. Each element ($J_{ex}^{Q}(j,j')$; (j=yz,zx,xy)) of the matrix representation of J_{ex}^{Q} is calculated as

$$J_{ex}^{Q}(j,j') = \delta_{\mathbf{k},\mathbf{k}'} \frac{16\pi^2}{45\Omega} k^2 \sum_{m_{1,2}=-2}^{2} (q_{m_1}^{*})_j (q'_{m_2})_{j'} \times Y_{2,m_1}^{*}(\theta,\phi) Y_{2,m_2}(\theta,\phi), \tag{18}$$

which leads to:

$$J_{ex}^{Q} \sim \sin^2\theta \cdot \begin{pmatrix} (\cos\theta\sin\phi)^2 & \cos^2\theta\cos\phi\sin\phi & \sin\theta\cos\theta\cos\phi\sin^2\phi \\ \cos^2\theta\cos\phi\sin\phi & (\cos\theta\cos\phi)^2 & \sin\theta\cos\theta\cos^2\phi\sin\phi \\ \sin\theta\cos\theta\cos\phi\sin^2\phi & \sin\theta\cos\theta\cos^2\phi\sin\phi & (\sin\theta\cos\phi\sin\phi)^2 \end{pmatrix}.$$

In terms of $\mathbf{k}$ and introducing the constant LR quadrupole-quadrupole exchange parameter Δ_Q, we obtain:

$$J_{ex}^{Q} = \Delta_Q \times \frac{1}{k^2}\begin{pmatrix} k_z^2k_y^2 & k_z^2k_xk_y & k_y^2k_zk_x \\ k_z^2k_xk_y & k_z^2k_x^2 & k_x^2k_yk_z \\ k_y^2k_zk_x & k_x^2k_yk_z & k_x^2k_y^2 \end{pmatrix}. \tag{19}$$

In contrast to dipole excitons, the LR part of the quadrupole-quadrupole exchange scales as $\mathbf{k}^2$ and is analytic at $k=0$. The first attempt to calculate this interaction was reported by Moskalenko, Bobyrysheva, and Kiselyova.[12] In their treatment the quadrupolar interaction between the exciton states was given as an effective dipole-dipole interaction, but did not take the off-diagonal interaction matrix elements into account. As these are of the same magnitude as the diagonal terms, this simplification is not justified.

B. Short-range exchange interaction

We now turn to the derivation of the SR exchange. The $\mathbf{K}_i \neq 0$ terms of Eq. (5) give the SR exchange, which we expand into orders of $\mathbf{k}$ and treat each order by the method of invariants.[1,13] This means that the Hamiltonian has to be invariant under the operations of the cubic symmetry group. The well-known $\mathbf{k}$-independent SR exchange splits the orthoexcitons from the paraexciton by $\Delta_0 = 12.1$ meV,[14] but leaves the orthoexcitons degenerate. The next higher-order term would scale linearly with $\mathbf{k}$. This term vanishes because of the inversion symmetry of the lattice (point group O_h). The SR exchange of order k^2 gives nonvanishing contributions: The electron and hole spin operators $\hat{\sigma}_e, \hat{\sigma}_h$ transform as Γ_4^+, while $\mathbf{k}$ is a polar vector and transforms as Γ_4^-. The direct product of the spin operators $\hat{\sigma}_e \otimes \hat{\sigma}_h$ and $\mathbf{k}\otimes\mathbf{k}$ terms are decomposed into the representations as follows:

$$\Gamma_4^+ \otimes \Gamma_4^+ = \Gamma_4^- \otimes \Gamma_4^- = \Gamma_1^+ \oplus \Gamma_3^+ \oplus \Gamma_4^+ \oplus \Gamma_5^+. \tag{20}$$

Consequently, the SR exchange $(\hat{\sigma}_e \otimes \hat{\sigma}_h)(\mathbf{k}\otimes\mathbf{k})$ is decomposed into contributions of Γ_1^+, Γ_3^+, Γ_4^+, and Γ_5^+ symmetry.[9] The operator part of total exchange Hamiltonian can be split into invariant representations H_i of symmetry Γ_i^+. To finally, obtain the exchange energies J_i we introduce the exchange parameters Δ_i.

Using the tables of Koster *et al.*[9] the exchange Hamiltonian of Γ_1^+ symmetry is given by

$$H_1 = \tfrac{1}{6}(2\hat{\sigma}_e \times \hat{\sigma}_h)(\mathbf{k}\cdot\mathbf{k}). \tag{21}$$

First, we will consider the spin operators in H_1:

$$2\hat{\sigma}_e \times \hat{\sigma}_h = 2\sigma_{e,z}\sigma_{h,z} + \sigma_{e,+}\sigma_{h,-} + \sigma_{e,-}\sigma_{h,+}, \tag{22}$$

with the standard momentum ladder operators $\sigma_{e/h,+}$, $\sigma_{e/h,-}$. Now we apply the spin operators to the electron-hole spin states of Eq. (13) and obtain

$$\begin{aligned} 2\hat{\sigma}_e \times \hat{\sigma}_h|S\rangle &= -\tfrac{3}{2}|S\rangle, \\ 2\hat{\sigma}_e \times \hat{\sigma}_h|T_0\rangle &= \tfrac{1}{2}|T_0\rangle, \\ 2\hat{\sigma}_e \times \hat{\sigma}_h|T_{+1}\rangle &= \tfrac{1}{2}|T_{+1}\rangle, \\ 2\hat{\sigma}_e \times \hat{\sigma}_h|T_{-1}\rangle &= \tfrac{1}{2}|T_{-1}\rangle. \end{aligned} \tag{23}$$

We apply the spin product operator to the orthoexciton states $|O_{yz}\rangle$, $|O_{zx}\rangle$, $|O_{xy}\rangle$

$$\begin{aligned} 2\hat{\sigma}_e \times \hat{\sigma}_h|O_{yz}\rangle &= \tfrac{1}{2\sqrt{6}}\phi_{c,s}[-3\sqrt{2}\phi_{v,yz}|S\rangle + \mathrm{i}\sqrt{2}\phi_{v,zx}|T_0\rangle \\ &\quad + \phi_{v,xy}(|T_{+1}\rangle + |T_{-1}\rangle)], \\ 2\hat{\sigma}_e \times \hat{\sigma}_h|O_{zx}\rangle &= \tfrac{-\mathrm{i}}{2\sqrt{6}}\phi_{c,s}[\sqrt{2}\phi_{v,yz}|T_0\rangle - \mathrm{i}3\sqrt{2}\phi_{v,zx}|S\rangle \\ &\quad + \phi_{v,xy}(|T_{+1}\rangle - |T_{-1}\rangle)], \\ 2\hat{\sigma}_e \times \hat{\sigma}_h|O_{xy}\rangle &= \tfrac{-1}{2\sqrt{6}}\phi_{c,s}[\phi_{v,yz}(|T_{+1}\rangle + |T_{-1}\rangle) - \mathrm{i}\phi_{v,zx}(|T_{+1}\rangle \\ &\quad - |T_{-1}\rangle) + 3\sqrt{2}\phi_{v,xy}|S\rangle]. \end{aligned} \tag{24}$$

The exchange matrix elements are given by:

$$\begin{aligned} \langle O_j|H_1|O_{j'}\rangle &= \tfrac{1}{6}\langle O_j|2\hat{\sigma}_e \times \hat{\sigma}_h \times (\mathbf{k}\cdot\mathbf{k})|O_{j'}\rangle \\ &= \tfrac{1}{6}\langle O_j|2\hat{\sigma}_e \times \hat{\sigma}_h|O_{j'}\rangle k^2. \end{aligned} \tag{25}$$

The Wannier functions are orthonormal $((\phi_{v,j}\cdot\phi_{v,j'}) = \delta_{j,j'})$, thus for $j=j'=yz$ we find

$$\langle O_{yz}|H_1|O_{yz}\rangle = \tfrac{-1}{36}k^2. \tag{26}$$

This holds for all diagonal elements. For $j \neq j'$ we find

$$\langle O_j|H_1|O_{j'}\rangle k^2 = 0. \tag{27}$$

The vanishing off-diagonal elements again reflect that the Γ_1^+ operator is spin conserving. As a consequence no mixing between the orthoexciton states occurs. The matrix representation of the SR exchange energy in the orthoexciton basis is thus given by:

$$J_1 = \Delta_1 \cdot \begin{pmatrix} k^2 & 0 & 0 \\ 0 & k^2 & 0 \\ 0 & 0 & k^2 \end{pmatrix} = \Delta_1 k^2 \cdot \mathbf{1}. \tag{28}$$

J_1 is proportional to the identity matrix and causes identical spectral shifts for all three orthoexciton states. Since J_1 scales as k^2 it contributes to the spatial dispersion where it can be interpreted as a correction to the effective mass. This will be discussed in detail in Sec. V. As Δ_1 does not give rise to an orthoexciton splitting it cannot be determined indepen-

dently in the current experiment. It is thus included in the energy E_0 of the degenerate orthoexciton states.

The exchange Hamiltonian of Γ_3^+ symmetry is given by:[9]

$$H_3 = \tfrac{1}{2\sqrt{2}}\Big[\tfrac{1}{3}(\hat{\sigma}_e\cdot\hat{\sigma}_h - 3\sigma_{e,z}\sigma_{h,z})(k^2-3k_z^2) + (\sigma_{e,x}\sigma_{h,x}-\sigma_{e,y}\sigma_{h,y}) \times (k_x^2-k_y^2)\Big]. \quad (29)$$

The exchange energies are again obtained by calculating the individual matrix elements, following the steps described in the treatment of H_1. We derive the matrix representation

$$J_3 = \Delta_3\begin{pmatrix} 3k_x^2-k^2 & 0 & 0 \\ 0 & 3k_y^2-k^2 & 0 \\ 0 & 0 & 3k_z^2-k^2 \end{pmatrix}. \quad (30)$$

Again, all off-diagonal elements vanish and no mixing of the basis states occurs. However, the **k**-dependence of the diagonal elements should give rise to an orthoexciton fine structure.

The Γ_4^+ electron-hole exchange obviously vanishes.

$$H_4 = \tfrac{1}{2\sqrt{3}}[(\sigma_{e,y}\sigma_{h,z}-\sigma_{e,z}\sigma_{h,y})(k_yk_z-k_zk_y) + (\sigma_{e,z}\sigma_{h,x}-\sigma_{e,x}\sigma_{h,z}) \times (k_zk_x-k_xk_z) + (\sigma_{e,x}\sigma_{h,y}-\sigma_{e,y}\sigma_{h,x})(k_xk_y-k_yk_x)] = 0. \quad (31)$$

Finally, the contribution of Γ_5^+ symmetry is given by:

$$H_5 = \tfrac{1}{\sqrt{3}}[(\sigma_{e,y}\sigma_{h,z}+\sigma_{e,z}\sigma_{h,y})(k_yk_z) + (\sigma_{e,z}\sigma_{h,x}+\sigma_{e,x}\sigma_{h,z})(k_zk_x) + (\sigma_{e,x}\sigma_{h,y}+\sigma_{e,y}\sigma_{h,x})(k_xk_y)] = \tfrac{1}{\sqrt{3}}[\Theta_{yz}(k_yk_z)+\Theta_{zx}(k_zk_x)+\Theta_{xy}(k_xk_y)]. \quad (32)$$

In analogy to the example of H_1 we again derive the action of the Γ_5^+ spin operators on the exciton states.

$$\Theta_{yz}|S\rangle = \Theta_{zx}|S\rangle = \Theta_{xy}|S\rangle = 0,$$

$$\Theta_{yz}|T_0\rangle = \tfrac{-i}{2\sqrt{2}}(|T_{+1}\rangle + |T_{-1}\rangle),$$

$$\Theta_{zx}|T_0\rangle = \tfrac{1}{2\sqrt{2}}(|T_{+1}\rangle - |T_{-1}\rangle),$$

$$\Theta_{xy}|T_0\rangle = 0,$$

$$\Theta_{yz}(|T_{+1}\rangle + |T_{-1}\rangle) = \tfrac{i}{\sqrt{2}}|T_0\rangle,$$

$$\Theta_{zx}(|T_{+1}\rangle + |T_{-1}\rangle) = 0,$$

$$\Theta_{xy}(|T_{+1}\rangle + |T_{-1}\rangle) = \tfrac{-i}{2}(|T_{+1}\rangle - |T_{-1}\rangle),$$

$$\Theta_{yz}(|T_{+1}\rangle - |T_{-1}\rangle) = 0,$$

$$\Theta_{zx}(|T_{+1}\rangle - |T_{-1}\rangle) = \tfrac{1}{\sqrt{2}}|T_0\rangle,$$

$$\Theta_{xy}(|T_{+1}\rangle - |T_{-1}\rangle) = \tfrac{i}{2}(|T_{+1}\rangle + |T_{-1}\rangle). \quad (33)$$

The Γ_5^+ operators give rise to a mixing among the triplet states. As the spin is not conserved, we expect only off-diagonal elements in the matrix representation. We find

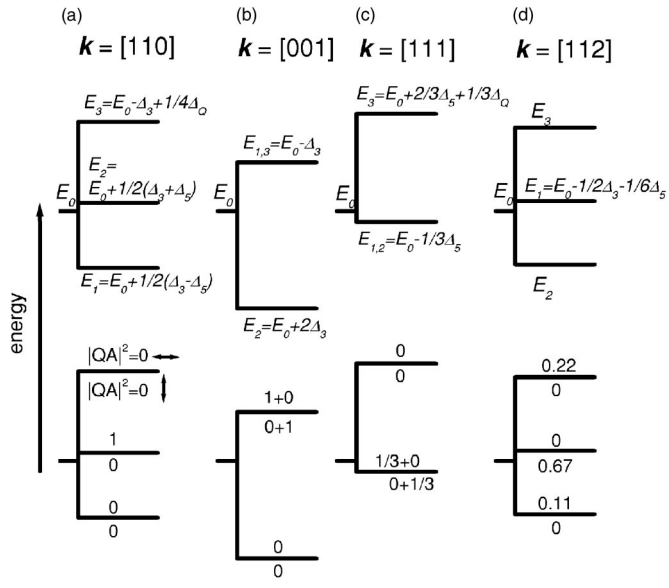

FIG. 1. Energy level diagram of the exciton fine structure. E_0 gives the orthoexciton energy including the exchange shifts Δ_0 and Δ_1. Panels (a), (b), (c), and (d) give the energy schemes for **k** =[110], [001], [111], and [112], respectively (Δ_Q=5 μeV, Δ_3= −1.3 μeV, Δ_5=2 μeV). In the upper schemes the analytic expressions for the exchange energy are indicated. For **k**=[112] the low symmetry gives rise to a rather complex analytic expression for E_2 and E_3. In the lower half the $|QA|^2$'s are given for each level. The upper and lower numbers correspond to horizontal and vertical polarization, respectively. In all cases the vertical axis is $[\bar{1}10]$.

$$J_5 = \Delta_5\cdot\begin{pmatrix} 0 & k_xk_y & k_xk_z \\ k_xk_y & 0 & k_yk_z \\ k_xk_z & k_yk_z & 0 \end{pmatrix}. \quad (34)$$

As for the LR term [Eq. (19)], a **k**-dependent mixing of the orthoexciton states is expected.

Summarizing, we have derived three electron-hole exchange terms of order k^2, that give rise to the orthoexciton fine structure: the LR quadrupole interaction J_Q^{ex} and the SR contributions J_3, J_5, where the absolute splittings are given by the exchange parameters Δ_Q, Δ_3, and Δ_5, which remain to be determined.

For high symmetry **k**'s (see Fig. 1) the matrices in Eqs. (19), (30), and (34) can be diagonalized analytically. The new eigenstates are linear combinations of $|O_{yz}\rangle$, $|O_{zx}\rangle$, and $|O_{xy}\rangle$. For **k** along [110], exchange should lift the degeneracy of the orthoexcitons and three separate lines are expected [Fig. 1(a)], where the E_2-E_1 splitting directly gives Δ_5. For **k** along [001] there is no contribution from J_{ex} and J_5. One thus expects a doubly degenerate level $E_{1,3}$ and a single level E_2 with a total splitting of $3\Delta_3$. In the [111] direction we expect to find a degenerate low energy state besides a single high energy level. For **k** along [112] we should again find three distinct orthoexciton energies.

For the detection of the fine structure the quadrupole amplitudes are crucial [Eq. (2)]. The lower part of Fig. 1 gives the $|QA_i|^2$'s for vertical and horizontal polarization. With the exception of the [112] direction, only one of the fine struc-

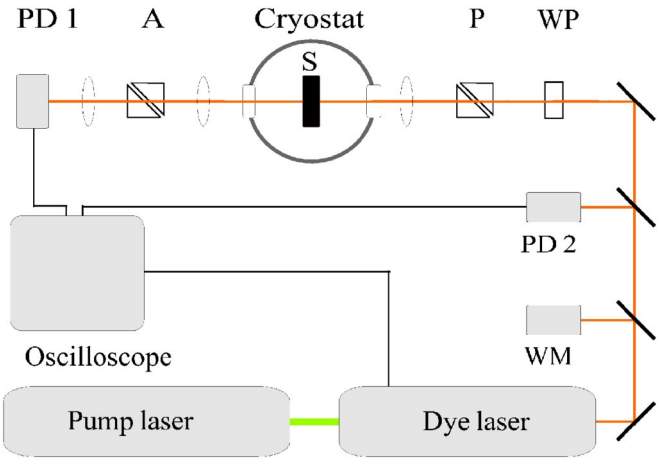

FIG. 2. (Color online) Schematic setup for high-resolution spectroscopy: *A*, analyzer; *P*, polarizer; *PD*, photodiode; *S*, sample; *WM*, wavelength meter; and *WP*, half wave plate.

ture components will be directly observable. It will be discussed below how to detect the other components.

III. EXPERIMENT

The **k**-dependence of the exchange is investigated in transmission experiments, where a laser beam propagating along **k**, directly probes the corresponding fine structure. Rotating the samples around the vertical axis gives access to intermediate **k**-directions. Such intermediate, lower symmetry **k**'s also break the strict polarization selection rules (compare Fig. 1). This leads to $|QA|^2 \neq 0$ for the fine structure components that are forbidden in high symmetry **k**'s. The dependence of the orthoexciton energies E_1, E_2, and E_3 on **k** can thus be measured.

Following these requirements, a setup for high-resolution absorption experiments (Fig. 2) has been designed. The crucial element is the tunable, frequency-stabilized, ring dye laser. The laser bandwidth of ≈ 2 neV gives access to a sub-μeV resolution. In the experiment the laser energy is continuously scanned across the orthoexciton resonance. The dye is excited by a frequency-doubled $Nd:YVO_4$-laser.

For rough adjustment of the laser energy, a wavelength meter with an accuracy of ≈ 2 μeV is used. The precision of the wavelength meter limits the absolute energy calibration of the setup. Therefore we will present spectra in terms of relative energies. The laser beam is passed through polarization optics (half-wave plate *WP* and polarizer *P*), to ensure precise control of the polarization of the exciting laser light. A lens focuses the laser beam onto a spot of about 30 μm on the sample. After passing through an analyzer (*A*) the transmitted photons are detected by photodiode 1, which is connected to an oscilloscope. Running the laser in the frequency scanning mode, the ramp voltage of the scan is used as trigger input for the oscilloscope. As the laser frequency is scanned, the transmittance of the specimen is monitored on the photodiode 1. Photodiode 2 is used as a reference, to compensate for intensity fluctuations of the laser source. Synchronizing the scan and the photodiode readout on the oscilloscope gives the spectrally resolved transmission. Typically, the scan range is set to ≈ 40 μeV with a scan time of 250 ms. The samples were mounted in a helium immersion cryostat, keeping them at a temperature of about 1.5 K.

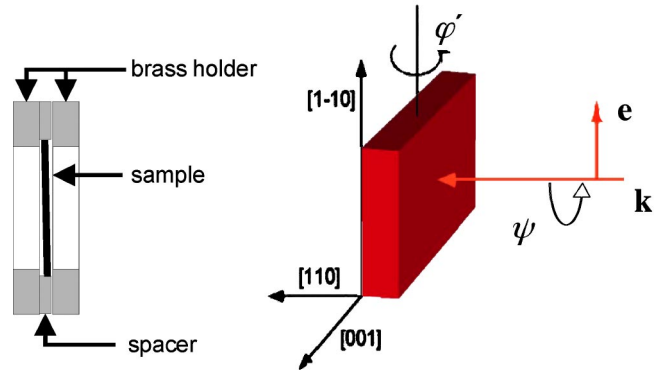

FIG. 3. (Color online) Left: Sample holder for strain-free mounting of thin Cu_2O slabs. Right: Configuration of angles φ' (rotation of the sample) and ψ (rotation of the polarization vector **e**).

High-resolution experiments are extremely sensitive to perturbations. One such perturbation is strain. Hence, great care was taken to mount the samples strain-free. In our experiments we used two types of samples. First, cube-shaped samples with dimensions of ≈ 4 mm. These samples were housed in a brass cage, slightly larger than the sample itself. Second, slab-shaped samples with lateral extensions of a few mm, while being only $d_S \lesssim 50$ μm thick. To ensure a strain-free upright mounting, special housings have been designed. The sample is sandwiched between two brass plates, while a spacer slightly thicker than the sample surrounds the specimen. A sectional drawing of such a holder is shown in Fig. 3.

The samples were cut from the same natural Cu_2O crystal and were oriented by X-ray diffraction. They were cut such that the surfaces correspond to a main crystalline axis (e.g., [001], [110], [111], [112]). After cutting, the surfaces were polished. This treatment can give rise to strain in the crystals. Samples showing signatures of strain were annealed. For this purpose they were heated up to 450 °C and slowly cooled in an evacuated tube. To reduce loss of oxygen, the samples were sandwiched between quartz plates.

The mounting allows the rotation of the sample around the vertical axis by an angle φ', which corresponds to an angle φ ($\sin\varphi = (\sin\varphi')/n_i$) for the laser beam inside the crystal. n_i is the index of refraction for the i'th polariton. Because of the extremely small oscillator strength of the quadrupole transitions, n_i can be approximated with high accuracy by $\sqrt{\epsilon_\infty} = 2.55$. As an example a crystal is shown where the rotation is around the $[1\bar{1}0]$ axis. Here for $\varphi = 0$ the light travels along [110]. For $\varphi \neq 0$ the light travels along intermediate **k**'s. By means of the polarization optics, **e** can be varied. The direction of **e** is given by the angle ψ (Fig. 3). $\psi = 0$ corresponds to horizontal **e**; in our example $\mathbf{e}(\psi = 0) = [001]$, while the vertical polarization $\psi = 90°$ corresponds to $\mathbf{e} = [1\bar{1}0]$.

The electron hole exchange for **k** along $[1\bar{1}0]$ is investigated in the experiments presented in Fig. 4, where the left

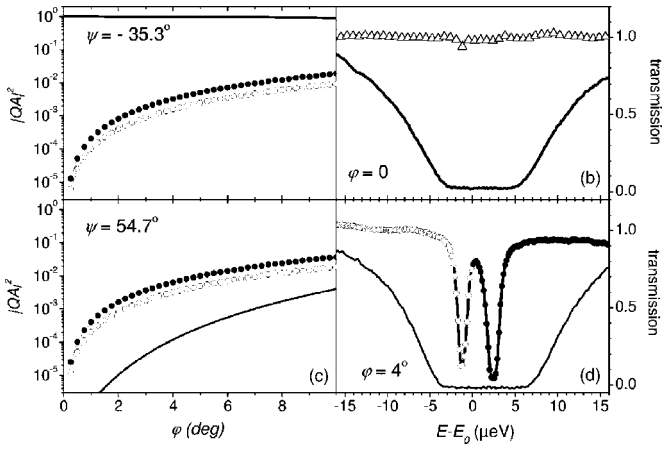

FIG. 4. (a) and (c) Calculated $|QA_1|^2$ (open symbols), $|QA_2|^2$ (full line), and $|QA_3|^2$ (full symbols) as a function of φ (rotation around the [111]-axis) for $\psi=-35.3°$ ($\mathbf{e}=[00\bar{1}]$ at $\varphi=0$) (a) and $\psi=54.7°$ ($\mathbf{e}=[110]$ at $\varphi=0$) (c). At $\varphi=0$ $\mathbf{k}$ is along $[\bar{1}10]$. (b) and (d) Transmission spectra of a 4-mm-thick crystal. (b) The full line gives the transmission spectra for $\psi=-35.3°$ and the triangles for $\psi=54.7°$ ($\varphi=0$). (d) Spectra for $\varphi=4°$ and $\psi=-35.3°$ (solid line) and $\psi=54.7°$ [open (full) dots correspond to E_1 (E_3)].

panels show the calculated transition amplitudes for $\psi=-35.3°$ 4(a) and $\psi=54.7°$ 4(c) as function of φ (rotation around the [111]-axis). Calculating $|QA_2|^2$ at $\mathbf{k}$ along $[\bar{1}10]$ ($\varphi=0$) shows that for $\psi=-35.3°$ ($\mathbf{e}(-35.3°)=[00\bar{1}]$) the transition E_2 is fully allowed, while E_1 and E_3 are forbidden [Fig. 4(a)]. In the corresponding experiment [solid line in Fig. 4(b)] one indeed finds a strong absorption. For $\psi=+54.7°$ ($\mathbf{e}(+54.7°)=[110]$) all three transitions are forbidden, as confirmed by the experiment [triangles in Fig. 4(b)]. This confirms the calculations of panel (a) and (c) and demonstrates the high crystallographic quality of the sample and the absence of symmetry breaking perturbations. The picture changes drastically if the sample is tilted slightly from $\varphi=0°$, where $\mathbf{k}$ no longer points exactly along $[\bar{1}10]$. For $\psi=-35.3°$, E_1 and E_3 gain oscillator strength for increasing φ, however E_2 remains almost fully allowed masking the two weak lines. As expected, the spectrum at $\varphi=4°$ shows only E_2. However, for $\psi=54.7°$ E_1 and E_3 are no longer covered by the E_2 transition, as $|QA_2|^2$ is about one order of magnitude smaller than $|QA_1|^2$ and $|QA_3|^2$. Indeed the orthoexciton doublet with an exchange splitting of 4 μeV is resolved [Fig. 4(d)].

The degeneracy of the orthoexciton is lifted. Besides the spectral signatures, we observe that the E_1 absorption is smaller than the E_2 absorption, as predicted [Fig. 4(c)]. Both lines are exceptionally narrow with a full width at half maximum of $\lesssim 1$ μeV. This gives further proof of the high quality of natural Cu_2O crystals and the small homogenous broadening of the quadrupole transition.

Having demonstrated qualitative agreement between theory and experiment, we proceed with the quantitative analysis of the three exchange parameters Δ_Q, Δ_3, and Δ_5. In our experiment $|\mathbf{k}|=k_0=2.62\times10^7$ m^{-1} is given by the intersection of the light cone with the exciton dispersion. As it is

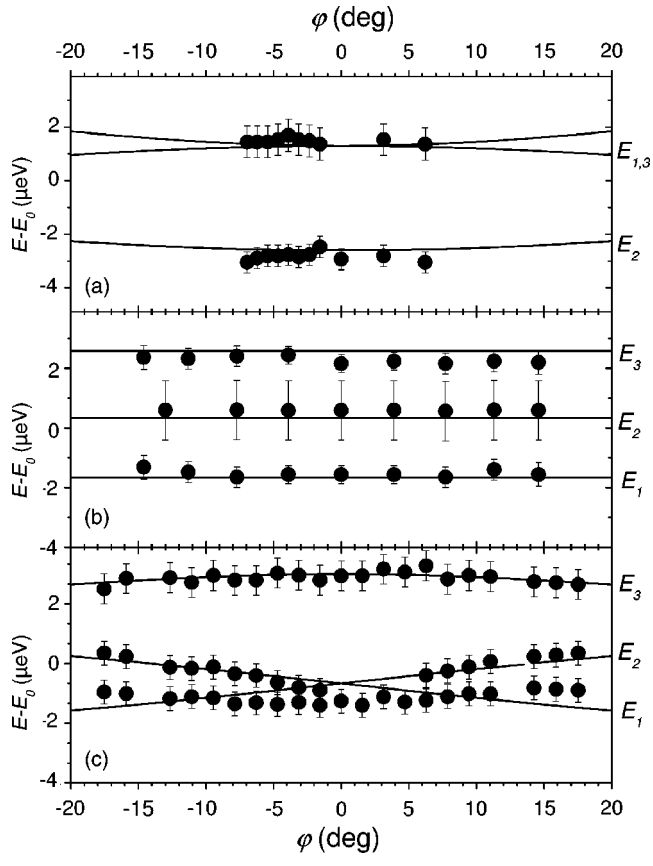

FIG. 5. E_1, E_2, and E_3 as a function of φ. Dots mark the experimental data. Full lines give the calculated values. (a) For $\varphi=0$, $\mathbf{k}$ is along [001]. φ describes a rotation around the $[1\bar{1}0]$-axis ($d_S=4$ mm). (b) For $\varphi=0$, $\mathbf{k}$ is along $[\bar{1}10]$. φ describes a rotation around the [111] axis ($d_S=4$ mm). (c) For $\varphi=0$, $\mathbf{k}$ is along [111]. φ describes a rotation around the $[11\bar{2}]$-axis ($d_S=85$ μm).

constant, we will treat $\mathbf{k}$ as a normalized unit-less vector. This allows us to directly express the exchange parameters as an exchange energy. For $\mathbf{k}$ along [001] [Fig. 5(a)] the fine structure is only determined by J_3, which allows to measure Δ_3 directly. The levels $E_{1,3}$ and E_2 are split by $3\Delta_3=3(-1.3)$ μeV (Fig. 1). In the angular range investigated no significant line shifts are expected and the degeneracy of E_1 and E_3 is only slightly lifted, which is masked by their spectral widths. For the sample orientation of Fig. 4, E_1, E_2, and E_3 are shown as a function of φ in Fig. 5(b). E_2-E_1 gives directly $\Delta_5=2$ μeV in the $\mathbf{k}=[\bar{1}10]$ configuration. Finally, $\Delta_Q=5$ μeV is determined from E_3. These parameters also give the correct relative line positions, when comparing the absolute energies obtained for $\mathbf{k}$ along [001] to those for $\mathbf{k}$ along $[\bar{1}10]$. The direct comparison of two measurements requires great care, as the absolute laser energy is not known with sufficient accuracy. Therefore, the experiments were performed with two samples mounted in the cryostat. While keeping the laser frequency stabilized, two consecutive measurements were performed on both samples that allows comparison of the relative exciton energies. The sample shown in Fig. 4 with the characteristic E_1-E_3 doublet was taken as spectral reference.

Now all exchange parameters have been measured close to **k**-directions of high symmetry. According to theory, these exchange parameters should apply for any arbitrary **k**. Hence, the crucial test for our description is done by measuring the exchange fine structure for **k**-directions with low symmetry. As a test of consistency we present data for **k** along [111] [Fig. 5(c)]. According to Fig. 1(c) we expect for $\varphi \rightarrow 0$ a degenerate level $E_{1,2}$ plus a high energy state E_3, where $|QA_3|^2$ should be much weaker than $|QA_{1,2}|^2$ ($\varphi \neq 0$). In panel (c) E_1, E_2, and E_3 are shown versus φ. The $E_1 - E_2$ splitting increases with $|\varphi|$, while E_3 shows only slight shifts. The fine structure is modelled (full lines) using the parameters obtained above. Obviously, Δ_Q, Δ_3, and Δ_5 allow a consistent description for these **k**'s. In samples of $d_S > 1$ mm, lines of large $|QA|^2$ become rather broad. This hinders the precise quantitative evaluation of the fine structure [see, e.g., error bar for E_2 in Fig. 5(b)]. To overcome this broadening a thin sample ($d_s = 30$ μm) had to be employed, which permits resolving the $E_1 - E_2$ splitting [Fig. 5(c)].

IV. IMPACT OF STRAIN

The degeneracy of the orthoexcitons could also be lifted by perturbations, such as strain.[15,16] Considering the energy scales we are dealing with, even slightest strain on the order of 1×10^3 N m^{-2} can cause a notable effect.[17] Two sources of strain have to be taken into account. First, external strain originating from the sample mounting. Our sample holders exclude this source. Second, the crystal itself can also be intrinsically strained. Such stress can originate from imperfections in the lattice structure, cutting and polishing during the sample preparation, or thermal stress. In the following we will evaluate to what extent this can influence our experiment findings.[18]

Let us first focus on cube-shaped samples with extensions of ≈4 mm. Because of the relatively large size of the specimen, an inhomogeneous strain distribution across the sample is expected. The central parts should be less affected by strain than the outer sections of the cube, where cutting and polishing can give rise to an increased stress. Hence, a strain-induced fine structure should depend on the sample section being probed.

To clarify this, the experiment of Fig. 4 was repeated for illumination of the specimen in the sample center (solid line in Fig. 6) and close to the sample edge (dotted line). Otherwise the experimental conditions are identical to those for the data given by the dots in Fig. 4. In both sections of the sample, two lines with a splitting of ≈4 μeV are found. The spectral shifts of E_1 and E_3 are insignificant as compared to the splitting. Additional spectra were recorded covering the entire surface area of the sample and the fine structure remained more or less unchanged. This indicates that the fine structure cannot be interpreted as being stress induced. A second argument along these lines is the following: In a thick sample a large volume is probed, even with a focused beam. Thus, inhomogeneous strain would give rise to an inhomogeneous broadening of the lines. However, for the laser beam passing through the sample center, the lines remain extremely narrow (FWHM ≤ 1 μeV) and Lorentzian in shape.

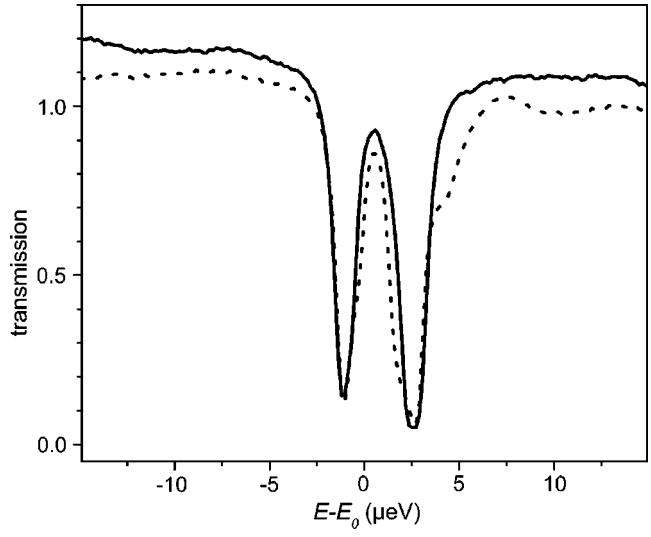

FIG. 6. Transmission spectra for $\varphi = 4°$ (rotation around the [111] axis and **k** along $[\bar{1}10]$ at $\varphi = 0$) and $\psi = 54.7°$. The spectra are recorded for excitation in the sample center (solid line) and excitation close to the edge of the sample (dashed line).

For the beam traveling along the edge of the sample, the line shape of E_3 deviates from a Lorentzian. The shoulder on the high-energy side might arise from a strained section of the sample. The data show that slight stress can be found in the surface regions of the sample. However, this does not have a significant impact on the fine structure and can be disregarded when the laser beam passes through the center of a thick sample.

The situation is more complex for thin samples of $d_s < 100$ μm. For such slab-shaped samples surface effects gain importance and stress-induced perturbations can no longer be disregarded a priori. Each sample has to be examined carefully. A first impression can be obtained via polarization microscopy: The crystal is placed between crossed polarizers. In a strain-free sample, the polarization of the transmitted light is unchanged and the light is blocked by the second polarizer. If the crystal is strained, the transmitted light becomes elliptically polarized and thus partly passes through the second polarizer. In Fig. 7 sections of two samples are shown. The sample on the left shows clear signatures of strain, which is inhomogeneous across the specimen. The picture on the right shows an homogenously

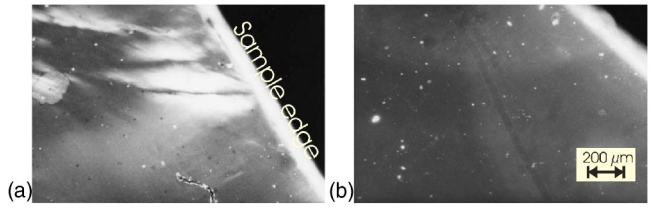

FIG. 7. Microscopic pictures of two slab-shaped samples. The specimens were positioned between two crossed polarizers. Hence, bright areas indicate where the sample is stressed. The bright white line is the sample edge. The dark areas in the upper right corners give a reference without sample. Both samples are about 100 μm thick.

weakly strained sample (the bright spots arise from dirt particles). Even if a crystal appears to be perfectly strain free under the polarization microscope, it does not mean that there is no residual strain. High-resolution spectroscopy provides a much more sensitive tool. Therefore each sample is tested for homogeneity by probing various sections of the specimen. Only if the spectral positions of the exciton resonances are independent of the sample section being probed, the specimen is suited for our purposes, even though this still does not prove that it is unstrained. It only shows that the strain induced perturbation is of the same magnitude as the $\mathbf{k}^2$ exchange and homogenous across the crystal.

As we still cannot exclude this perturbation, we have to clarify how such residual strain affects the orthoexciton fine structure. The impact of strain can be approached by symmetry considerations: The strain tensors possess the same symmetry as the SR $\mathbf{k}^2$-exchange terms.[1,2] Therefore the effect of strain on $|O_{yz}\rangle$, $|O_{zx}\rangle$, and $|O_{xy}\rangle$ is described by the same types of symmetry operators as given in Eqs. (28), (30), and (34). Replacing $k_i k_j (i,j=x,y,z)$ by the corresponding elements ϵ_{ij} of the strain tensor we find

$$S_1 = \delta_1 \cdot \begin{pmatrix} \epsilon_{xx}+\epsilon_{yy}+\epsilon_{zz} & 0 & 0 \\ 0 & \epsilon_{xx}+\epsilon_{yy}+\epsilon_{zz} & 0 \\ 0 & 0 & \epsilon_{xx}+\epsilon_{yy}+\epsilon_{zz} \end{pmatrix}, \tag{35}$$

$$S_3 = \delta_3 \cdot \begin{pmatrix} 2\epsilon_{xx}^2-\epsilon_{yy}^2-\epsilon_{zz}^2 & 0 & 0 \\ 0 & 2\epsilon_{yy}^2-\epsilon_{xx}^2-\epsilon_{zz}^2 & 0 \\ 0 & 0 & 2\epsilon_{zz}^2-\epsilon_{xx}^2-\epsilon_{yy}^2 \end{pmatrix}, \tag{36}$$

$$S_4 = 0;\ S_5 = \delta_5 \cdot \begin{pmatrix} 0 & \epsilon_{xy} & \epsilon_{xz} \\ \epsilon_{xy} & 0 & \epsilon_{yz} \\ \epsilon_{xz} & \epsilon_{yz} & 0 \end{pmatrix}. \tag{37}$$

Hence, the stress can be quantified by three parameters δ_1, δ_3, and δ_5, where S_1 simply shifts all three states, and S_3 and S_5 give rise to splittings. However, strain-induced shifts can be discriminated from exchange as they are fixed to the lattice and hence depend only on the orientation of the crystalline axes, but not on $\mathbf{k}$. Therefore, when probing various $\mathbf{k}$'s (turning the crystal) one would not expect any dependence of the energy levels on φ for strain-induced effects.

In Fig. 8, the spectral positions of the orthoexciton resonances are studied versus φ with $\mathbf{k}=[111]$ at $\varphi=0$ and rotation around $[11\bar{2}]$. In panel (a) the exchange splittings according to the parameter set obtained above are shown (solid traces). Apparently the calculations do not match the data, as the $E_{1,2}$-E_3 splitting is by a factor of two too large in the experiment. The experiments also show an asymmetry with respect to $\varphi=0$. The data seem to be shifted towards lower angles by about 2°. Nevertheless, we find the qualitative structure as known from Fig. 5(c). In panel (b) the calculations include strain of Γ_3^+ and Γ_5^+ type ($\delta_1=0$), while the exchange parameters remain unaltered. When neglecting the exchange induced shifts, we end up with constant energy

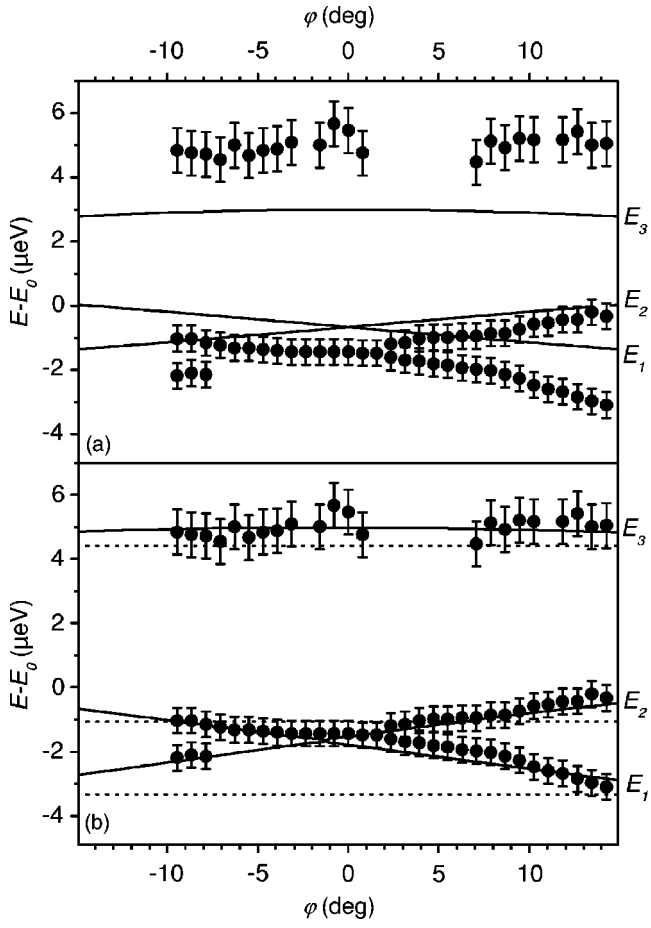

FIG. 8. Orthoexciton energies as function of φ (rotation around the $[11\bar{2}]$ axis) for $d_S=30$ μm ($\mathbf{k}=[111]$ at $\varphi=0$). The experimental data are given by full dots. In panel (a) calculations for the parameters $\Delta_Q=5$ μeV, $\Delta_5=2$ μeV, and $\Delta_3=-1.3$ μeV are plotted (solid lines). In panel (b) the calculations (solid lines) also include strain of Γ_3^+ ($\delta_3=-1.4$ μeV) and Γ_5^+ ($\delta_5=-2.1$ μeV) type, keeping the exchange parameters fixed. The dashed lines give the strain offsets.

levels [dashed lines in Fig. 8(b)]. As evident from this modeling, the φ ($\mathbf{k}$) dependence solely arises from exchange, while the increased splittings arise from residual strain. Most convincingly, the $\mathbf{k}$ dependence is again very well described by the set of exchange parameters derived above. The inclusion of strain also gives the explanation for the shift toward lower φ observed in the data set. It simply originates from strain offsets.

As a final test for the wave vector dependence of electron-hole exchange, we proceed with a $\mathbf{k}$ of even lower symmetry. For this crucial experiment we have chosen a crystal with $\mathbf{k}$ along $[11\bar{2}]$ at $\varphi=0$. The experimental findings are shown in Fig. 9, where the upper panels show spectra for the two polarizations $[\bar{1}10]$ 9(a) and [111] 9(b). For all $\mathbf{k}$'s we have access to all fine structure components with comparable $|QA|^2$'s [see Fig. 1(d)]. Panel (c) shows the φ-dependence of the orthoexciton energies. Including slight strain offsets again gives a good agreement between theory and experiment. Especially the characteristic $\mathbf{k}$ dependence is well described by the exchange parameters. As the exchange param-

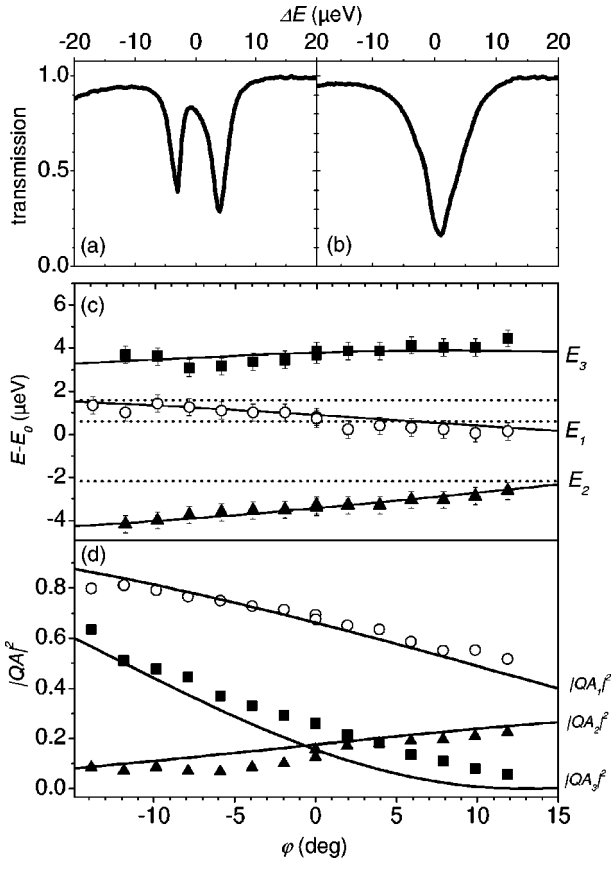

FIG. 9. Transmission spectra at $\mathbf{k}=[11\bar{2}]$ ($d_S=95$ μm) for $\psi=0$ ($\mathbf{e}=[111]$) (a) and $\psi=90°$ (b) ($\mathbf{e}=[\bar{1}10]$). (c) Orthoexciton energies as function of φ ($\mathbf{k}=[11\bar{2}]$ at $\varphi=0$, axis of rotation $[\bar{1}10]$). Squares correspond to E_3, open dots to E_1, and triangles to E_2. Calculations based on the parameters $\Delta_Q=5$ μeV, $\Delta_5=2$ μeV, $\Delta_3=-1.3$ μeV, $\delta_3=0.7$ μeV, and $\delta_5=1.0$ μeV are plotted as solid lines. The strain offsets are given by dotted lines. (d) $|QA_i|^2$'s as function of φ. Solid traces give the calculated $|QA_i|$'s.

eters determine the mixing between $|O_{yz}\rangle$, $|O_{zx}\rangle$, and $|O_{xy}\rangle$, they also influence the corresponding quadrupole amplitudes. In panel (d) the measured $|QA|^2$'s are compared to the calculations and we find very good agreement.

V. INFLUENCE ON THE EFFECTIVE EXCITON MASS

As the exchange terms discussed here scale quadratically in **k**, they can also be interpreted in terms of a **k**-dependent effective mass. Naturally, previous measurement of the exciton mass M have not taken these contributions into account. As we have seen, the exchange shifts are on the order of few μeV and hence comparable to the kinetic energy of the exciton at the exciton-photon resonance k_0. The wave-vector-dependent contributions to the effective mass are thus not negligible. In the following, we will evaluate how exchange-induced contributions to the exciton mass affect such measurements.

As pointed out already by Yu and Shen,[19,20] there is a discrepancy between the effective exciton mass M_0 derived from the band masses of the conduction band m_e and the valence band m_h ($M_0=m_e+m_h$) and the mass derived from resonant Raman experiments. From the latter the authors obtain $M=(3.0\pm0.2)$ m_0, with the free electron mass m_0. From cyclotron resonance experiments Goltzene and Schwab find the band masses $m_e=0.98$ m_0 and $m_h=0.66$ m_0.[21] Assuming the crystals in the resonant Raman experiments were oriented along the $\mathbf{k}=[001]$, their results have to be interpreted as follows: Looking at Fig. 1(b) we find that only the $E_{1,3}$ level is optically allowed, which means that the investigated orthoexciton is shifted by $-\Delta_3$ from E_0. As mentioned above E_0 already includes the SR exchange of Γ_1^+ symmetry with the exchange energy Δ_1.

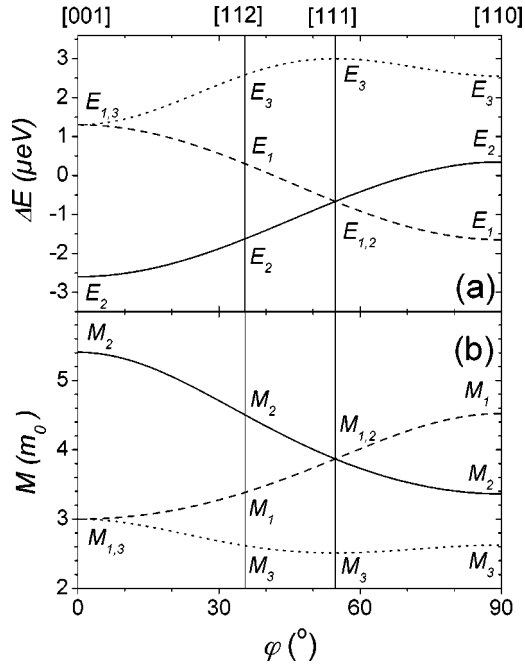

FIG. 10. (a) Exchange shifts of the orthoexcitons as function of φ. **k** lies in the [001]-[110] plane. (b) Effective exciton mass as function of φ.

When calculating the effective exciton mass for $\mathbf{k}=[001]$, the Γ_1^+ and Γ_3^+ terms have to be included. The effective mass $M_{1,3}$ of the $E_{1,3}$ resonance is then given by

$$\frac{\hbar^2 k_0^2}{2M_{1,3}} = \frac{\hbar^2 k_0^2}{2M_0} + \Delta_1 - \Delta_3. \tag{38}$$

From resonant Raman scattering we know that $M_{1,3}$ equals (3.0 ± 0.2) m_0.[19,20] As we also know the individual masses of the exciton constituents, we can now determine $\Delta_1=-8.6$ μeV. Δ_1 is of the same magnitude as the other exchange parameters. Taking the exchange into account the controversial reports on the exciton mass can be explained in a straight forward way. The exchange interaction between the exciton constituents gives thus rise to an effective mass different from the sum of the electron and hole masses. However, there might be additional reasons for this difference.[22]

Obviously the **k**-dependence of the exchange gives rise to an anisotropy of the effective mass. Using Eq. (38) and knowing the exchange shift from E_0 and Δ_i we can now calculate the mass M_i as function of **k**:

$$\frac{1}{M_i(\mathbf{k})} = \frac{1}{M_{1,3}(\mathbf{k}=[001])} + \frac{2}{\hbar^2 k_0^2}(\Delta_3 + \Delta_i(\mathbf{k})). \quad (39)$$

Figure 10(b) shows the exciton masses for the **k**-directions in the [001]-[110] plane. Indeed the anisotropy is significant. For example at $\mathbf{k}=[001]$ the effective mass of the two orthoexcitons differs by almost a factor of two.

VI. CONCLUSIONS

We have derived and demonstrated k^2-dependent electron-hole exchange interaction. For the yellow 1S orthoexcitons in Cu_2O the exchange parameters $\Delta_Q=5\ \mu$eV, $\Delta_1=-8.6\ \mu$eV, $\Delta_3=-1.3\ \mu$eV, and $\Delta_5=2\ \mu$eV are obtained. The k^2-dependent exchange is interpreted as an interaction-induced correction to the effective mass. The magnitude of this correction is of the same order as the kinetic energy at k_0. Our results explain the discrepancies found in the measurements of the effective-exciton mass and the masses of its constituents. The exchange parameters apply only for this specific exciton transition, however the k^2-dependent exchange is a fundamental property. Even though this effect has not been observed before, it should be present for all exciton transitions. The theoretical approach presented here is semi-empirical and the magnitude of the exchange parameters is only accessible experimentally. We hope that our experiments motivate microscopic calculations of the higher-order exchange terms.

ACKNOWLEDGMENTS

The work was supported by the Deutsche Forschungsgemeinschaft and the QuIST program of DARPA. We thank G. Baldassarri Höger von Högersthal for fruitful discussions and M. Kulka for providing a program for the data acquisition.

*Present address: Laboratoire Pierre Aigrain, École Normale Supérieure, 24, rue Lhomond, F-75005 Paris, France. Electronic address: gregor.dasbach@lpa.ens.fr

[1] K. Cho, Phys. Rev. B **14**, 4463 (1976).
[2] G. L. Bir and G. E. Pikus, *Symmetry and Strain-Induced Effects in Semiconductors* (John Wiley and Sons, New York, 1974).
[3] E. L. Ivchenko and G. E. Pikus, *Superlattices and Other Heterostructures* (Springer-Verlag, Berlin, 1995).
[4] M. Bayer, G. Ortner, O. Stern, A. Kuther, A. A. Gorbunov, A. Forchel, P. Hawrylak, S. Fafard, K. Hinzer, T. L. Reinecke, S. N. Walck, J. P. Reithmeier, F. Klopf, and S. Schäfer, Phys. Rev. B **65**, 195315 (2002).
[5] U. Rössler and H. R. Trebin, Phys. Rev. B **23**, 1961 (1981).
[6] H. Fu, L.-W. Wang, and A. Zunger, Phys. Rev. B **59**, 5568 (1999).
[7] G. Dasbach, D. Fröhlich, H. Stolz, R. Klieber, D. Suter, and M. Bayer, Phys. Rev. Lett. **91**, 107401 (2003).
[8] V. T. Agekyan, Phys. Status Solidi A **43**, 11 (1977).
[9] G. F. Koster, J. O. Dimmock, R. G. Wheeler, and H. Statz, *Properties of the Thirty-Two Point Groups* (M.I.T. Press, Cambridge, MA, 1963).
[10] R. J. Elliott, Phys. Rev. **124**, 340 (1961).
[11] J. S. Schwinger, L. L. J. Deraad, K. A. Milton, W.-Y. Tsai, and J. Schwinger, *Classical Electrodynamics* (Perseus Books, Reading, MA, 1998).
[12] S. A. Moskalenko, A. I. Bobyrysheva, and E. S. Kiselyova, Phys. Status Solidi B **213**, 377 (1999).
[13] J. M. Luttinger, Phys. Rev. **102**, 1030 (1956).
[14] G. Kuwabara, M. Tanaka, and H. Fukutani, Solid State Commun. **21**, 599 (1977).
[15] H. R. Trebin, H. Z. Cummins, and J. L. Birman, Phys. Rev. B **23**, 597 (1981).
[16] R. G. Waters, F. H. Pollak, R. H. Bruce, and H. Z. Cummins, Phys. Rev. B **21**, 1665 (1980).
[17] K. Reimann and K. Syassen, Phys. Rev. B **39**, 11113 (1989).
[18] G. Dasbach, D. Fröhlich, H. Stolz, R. Klieber, D. Suter, and M. Bayer, Phys. Status Solidi B **238**, 541 (2003).
[19] P. Y. Yu and Y. R. Shen, Phys. Rev. Lett. **1974**, 939 (1974).
[20] P. Y. Yu and Y. R. Shen, Phys. Rev. B **12**, 1377 (1975).
[21] A. Gotzene and C. Schwab, Solid State Commun. **18**, 1565 (1976).
[22] G. M. Kavoulakis, Y.-C. Chang, and G. Baym, Phys. Rev. B **55**, 7593 (1997).